A MODEL OF EPITHELIAL WATER TRANSPORT

THE CORNEAL ENDOTHELIUM

LARRY S. LIEBOVITCH, *Columbia University, College of Physicians and Surgeons, Department of Ophthalmology, New York 10032*

SHELDON WEINBAUM, *The City College of the City University of New York, Department of Mechanical Engineering, New York 10031*

ABSTRACT To try to understand how an epithelial tissue can transport water between bathing solutions of equal tonicity and how intracellular solute and protein concentration are related to the structural specialization of the cell membrane at its apical, basal, and lateral margins, we have formulated and solved, using approximate analytical techniques, a new model which combines the detailed transport of local osmotic flow in the extracellular channel with the multicompartment approach of thermodynamic models requiring the overall conservation of water and solute for the entire cell layer. Thus, unlike most previous models, which dealt exclusively with either the average properties of the cell layer or the local transport in the extracellular channel, we are able to solve simultaneously for the interaction of the cell with its environments across its apical, basal, and lateral cell membranes as well as the detailed transport in the extracellular channel. The model is then applied to corneal endothelium to obtain new insight into the water flow movement in this tissue under in vitro and in vivo conditions. The in vitro solution shows that the cell at 297 mosmol/liter is slightly hypotonic to the 300-mosmol/liter external bathing solutions which drive water equally out both the aqueous (apical) and stromal (basal) cell faces. This water is replaced from the extracellular channel. There is a net flow of water because more water enters the channel through its open stromal end than through the higher resistance tight junction. In vivo, the solution predicts that the stromal swelling pressure forces water through the tight junctions towards the stroma so that there is no net flow. The interesting new features of our solution are the water recirculation pattern and the role of the osmotically active proteins in making the cell hypertonic relative to the channel.

INTRODUCTION

Epithelial membranes have the important ability to transport solute and water between bathing solutions that are isotonic or even have hydrostatic and electrochemical gradients counter to the direction of flow (1–3). Theories to explain the flows of solute and water across epithelia can be divided into two general types which Skadhauge (4) has aptly characterized as "thermodynamic" or "microscopic."

The thermodynamic models use the nonequilibrium thermodynamic analysis developed by Kedem and Katchalsky (5, 6). The advantage of this formulism is that it guarantees that complete and consistent equations can be formulated that describe the integrated average flows of solutes and water across the entire tissue layer. The drawback of this formulism is that the thermodynamic parameters cannot be related to the tissue microstructure or the local solute and water fluxes since each region is homogeneous. The first model of this type was the

three-compartment model introduced by Curran (7). Curran's analysis was extended by Patlak et al. (8) and related in detail to the gallbladder by Kaye et al. (9). These models treat the tissue as divided into three homogeneous compartments separated by two limiting membranes in series. Net fluid transport is accomplished by osmotic forces driving water across one relatively impermeable membrane and hydrostatic forces driving water across the other relatively permeable membrane. Sometimes a paracellular shunt is included as a fourth homogenous compartment as in the model by Spring (10). These early thermodynamic models neglect the exchange of solute and water between the cell and the extracellular channel. The more recent thermodynamic model of Sackin and Boulpaep (11, 12) does include the lateral membrane fluxes for water and solute and also extends the analysis to more than one ion, but requires the basal cell membrane to be completely impermeable to ions and water. Thus, none of the existing models simultaneously treat the flows of solute and water across the apical, basal, and lateral cell membranes. Furthermore, all these models assume that the extracellular channel is a well-mixed homogeneous compartment.

In contrast to the homogeneous-compartment models described above, the microscopic models do calculate the local concentration gradients in the extracellular spaces between the cells. However, the drawback of existing microscopic models is that they are limited to a treatment of just these extracellular channels and do not couple this flow to the solute and water movement across the apical and basal faces of the cell. The first of these microscopic models was the standing gradient model formulated by Diamond and Bossert (13, 14) for extracellular channels closed at one end. Their analysis was extended to include more general exit boundary conditions by Weinbaum and Goldgraben (15), and Sackin and Boulpaep (11, 12). The analysis was further extended to include the flows of several ions (16–21). None of the existing models have considered the intracellular protein concentration in determining the overall water-flux balance on the cell. The basic premise of these local standing gradient models is that the local solute concentration differences osmotically drive water from the cell into the extracellular channel. This flow of water increases the hydrostatic pressure within the channel, forcing water out of the open channel mouth. In some tissues, however, the water flow may be due to differences in the reflection coefficients of different ions at the tight junction (16, 17) or net osmotic (18, 19) or hydrostatic (22) pressure gradients across the epithelial cell layer. Although some of these recent microscopic models deal in a very sophisticated way with the flows along the extracellular channel, none of them require that the net water flow entering the channel from the cell be equal to the net water flow into the cell across the apical and basal cell membranes. Hence, such models cannot adequately predict the concentrations of both ionic solutes and proteins within the cell.

In summary, the thermodynamic models adequately deal with the flows of solute and water across the apical and basal faces of the cell but inadequately represent the extracellular channel as a homogeneous compartment. The microscopic models adequately deal with the gradients of concentration and hydrostatic pressure within the extracellular channel but inadequately treat the flows across the apical and basal faces of the cell and thus cannot be used to determine the ionic solute and protein concentrations within the cell. Therefore, we have tried to formulate a new model representing a synthesis of the thermodynamic and microscopic viewpoints that simultaneously considers both the flows across the apical and basal faces of the cell and the detailed transport and gradients in the extracellular channel.

Furthermore, we shall develop approximate analytic solution procedures for obtaining closed form solutions to this more complicated model and illustrate its application by considering the corneal endothelium in detail.

FORMULATION OF THE GENERAL MODEL

Fig. 1 is a schematic illustration of the individual cells in a monolayered epithelium of hexagonally arranged cells showing the pertinent ultrastructural dimensions and physical parameters describing a rather general transport situation. The extracellular channel, of length L_2 and width h_2 is capped at the apical end by a tight junction length L_1 and width h_1. There are two contributions to the total concentration of particles within the cell: C_c, a single species of mobile solute that can be driven across the cell membrane by active transport or diffusion down its concentration gradient; and A_c, an impermeant species such as cellular proteins which are unable to cross the cell membrane. The cell is surrounded on its lateral, apical, and basal margins by differing concentrations of permeable extracellular solute $C(x)$, Γ_1, and Γ_2. The reflection coefficient for this solute is assumed to be unity through the cell membrane and σ_{TJ} through the tight junction. We also allow for a concentration Z_1, in the apical bathing solution of a solute impermeant to the cell membrane and tight junction. The

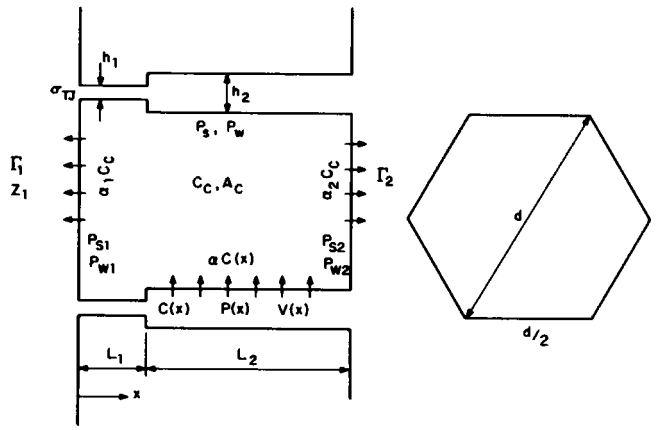

FIGURE 1

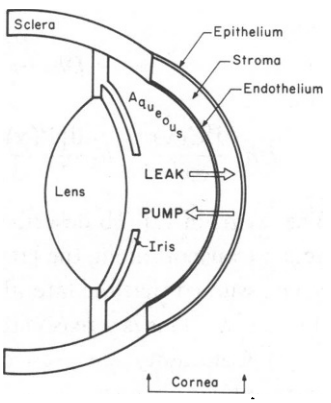

FIGURE 2

FIGURE 1 Transverse and face-on views of an epithelium composed of a single cell layer showing the model parameters described in the text. Inside the cell are indicated the cell membrane permeant solute concentration C_c and the cell membrane impermeant protein concentration A_c. Inside the extracellular channel are indicated the solute concentration $C(x)$, hydrostatic pressure $P(x)$, and fluid velocity $V(x)$. The cell membrane permeant solute concentration in the apical and basal solution are Γ_1 and Γ_2. The reflection coefficient for that solute across the tight junction is σ_{TJ}. There is also concentration Z_1 of another solute impermeant to both the cell and membrane and tight junction in the apical solution. The lateral, apical, and basal cell membranes have solute permeabilities P_s, P_{s1}, and P_{s2} and water permeabilities P_w, P_{w1}, and P_{w2}. Solute pumps translocate $\alpha C(x)$, $\alpha_1 C_c$, and $\alpha_2 C_c$ moles of solute per second across each cm^2 of cell membrane. (The direction of solute pumping shown is that for our model of the corenal endothelium which is classified as a backward fluid transporting epithelium because fluid flow is towards the tight junctions.)

FIGURE 2 Stylized drawing of the gross anatomy of the eye. The fluid from the aqueous chamber that leaks into the corneal stroma is removed by the fluid pump of the corneal endothelium.

lateral, apical, and basal cell membranes have solute permeabilities P_s, P_{s1}, and P_{s2}; and water permeabilities P_w, P_{w1}, and P_{w2}. Solute pumps with strength proportional to the local solute concentration are located on the lateral, apical, and basal cell membranes so that the solute fluxes per centimeter^2 of cell membrane are $\alpha C(x)$, $\alpha_1 C_c$ and $\alpha_2 C_c$. (For a "backward" fluid transporting epithelium, such as the corneal endothelium, where fluid is transported toward the apical face of the cell, the direction of solute pumping is as shown in Fig. 2.)

In the following mathematical model, we assume that the cell and tight-junction geometry (d, h_1, L_1, h_2, L_2), the pump constants (α, α_1, α_2), the cell membrane solute and water permeabilities (P_s, P_{s1}, P_{s2}, P_w, P_{w1}, P_{w2}), the pressure (P_1, P_2) and concentrations of solute (Γ_1, Γ_2) and impermeant solute (Z_1) in the bathing solutions are also prescribed. Given representative input values for all these parameters, we wish the model to predict the intracellular concentrations of solute and proteins (C_c, A_c), the spatial distributions of solute, hydrostatic pressure and velocity in the channel [$C(x)$, $P(x)$, $V(x)$], and the detailed distribution of the water and solute fluxes along the entire perimeter of the cell. The model at this time does not attempt to relate the geometry of the extracellular channel to the passively induced pressure field generated by the water movement.

The above problem formulation requires that one has a sufficient number of equations and associated boundary conditions to determine the five unknowns: C_c, A_c, $C(x)$, $P(x)$, and $V(x)$. Below are the fundamental conservation equations to determine these five variables.

(*a*) Transport of solute along the tight junction and extracellular channel:

$$-Dh_1 \frac{d^2C(x)}{dx^2} + h_1 \frac{d[V(x)C(x)]}{dx} = 0 \qquad 0 \le x \le L_1 \tag{1a}$$

$$-Dh_2 \frac{d^2C(x)}{dx^2} + h_2 \frac{d[V(x)C(x)]}{dx} = -2P_s[C(x) - C_c] - 2\alpha C(x) \quad L_1 \le x \le L_1 + L_2 \tag{1b}$$

The terms in Eq. 1b describe channel diffusion, convection, and the passive solute leak and active transport along the lateral membrane, in that order. For mathematical convenience we have assumed that the lateral cell membrane is impermeant to solute along the tight junction $0 \le x \le L_1$. This is a reasonable simplification when $L_1 \ll L_2$.

(*b*) Continuity equation coupling the movement of water to or from the cell into the extracellular channel:

$$h_1 \frac{dV(x)}{dx} = 0 \qquad 0 \le x \le L_1 \tag{2a}$$

$$h_2 \frac{dV(x)}{dx} = 2P_w[C(x) - (C_c + A_c)] \qquad L_1 \le x \le L_1 + L_2. \tag{2b}$$

Eq. 2b relates the change in the average fluid velocity along the channel to the fluid flow osmotically induced across the lateral membrane. In Eq. 2a we have assumed that the lateral cell membrane is also impermeant to water along the tight junction.

(*c*) Momentum equation to determine the pressure variation in the extracellular channel:

$$P(x) - P(0) = -\int_{x=0}^{x} \frac{12\mu V(x)}{h_1^2}\, dx \qquad 0 \le x \le L_1 \tag{3a}$$

$$P(x) - P(0) = -\int_{x-0}^{L_1} \frac{12\mu V(x)}{h_1^2}\,dx - \int_{x-L_1}^{x} \frac{12\mu V(x)}{h_2^2}\,dx \qquad L_1 \le x \le L_1 + L_2. \quad (3b)$$

Here μ is the absolute viscosity and we have used the hydrodynamic equation for Poiseulle flow between parallel plates.

(*d*) Solute conservation equation requiring that the amount of solute entering the cell equals the amount leaving the cell:

$$S_1\alpha_1 C_c + S_1 P_{s1}(C_c - \Gamma_1) + S_2\alpha_2 C_c + S_2 P_{s2}(C_c - \Gamma_2) - \int_{x-L_1}^{L_1+L_2} \ell\alpha C(x)dx + \int_{x-L_1}^{L_1+L_2} \ell P_s[C_c - C(x)]dx = 0. \quad (4)$$

The surface areas of the apical and basal cell membranes are given by S_1 and S_2; perimeter of the cell in a plane parallel to the apical and basal surfaces is given by ℓ. The first four terms in Eq. 4 describe the active transport and passive solute leak along the apical and basal surfaces whereas the last two terms represent these same integrated fluxes along the lateral membrane. The lateral pump strength constant α is defined to be positive when solute is pumped in the direction shown in Fig. 1.

(*e*) Water conservation equation requiring that the amount of water entering the cell equals the amount leaving the cell:

$$S_1 P_{w1}[\Gamma_1 + Z_1 - (C_c + A_c)] + S_2 P_{w2}[\Gamma_2 - (C_c + A_c)] + \int_{x-L_1}^{L_1+L_2} \ell P_w[C(x) - (C_c + A_c)]dx = 0. \quad (5)$$

Eq. 5 relates the passive water fluxes across the apical and basal surfaces to that across the lateral membranes. This equation can also be rewritten as

$$C_c + A_c = [S_1 P_{w1}/(SP)_T](\Gamma_1 + Z_1) + [S_2 P_{w2}/(SP)_T]\Gamma_2 + [SP_w/(SP)_T](1/L_2)\int_{x-L_1}^{L_1+L_2} C(x)dx \quad (6)$$

where the surface areas of the lateral, apical, and basal cell membranes are given by S, S_1, S_2 and $(SP)_T = S_1 P_{w1} + S_2 P_{w2} + SP_w$. Note that $1/L_2 \int C(x)dx$ is the average solute concentration in the extracellular channel. In other words, in a steady state, the total intracellular concentration $C_c + A_c$ equals the average of the environmental concentrations surrounding the cell weighted by the cell membrane water permeability and area facing each concentration. If this condition is not met, there will be a transient flow of water into or out of the cell, changing its volume and concentration until the condition is satisfied.

It is in the inclusion of both Eqs. 4 and 5, which relate that intracellular and extracellular environments, that the present formulation differs substantively from previous microscopic models.

One assumption implicit in the previous discussion is that the intracellular salt concentration is uniform. In an earlier, less complete, version of the new mathematical model (23), it was demonstrated through a perturbation analysis that small intracellular concentration gradients do exist (otherwise the actively transported salt ion would not be replenished at active transport sites) but that these gradients within the cell are (h_2/d) smaller than those within the channel. This is because the physically relevant length scale for diffusional mixing

in the channel is the channel width h_2, which is much less than the channel length L_2, while the relevant length scale for mixing in the cell is the cell width d which is of the same order as the cell length L_2. These same arguments apply to the pressure field and the fluid velocity within the cell. The water flow velocity inside the cell is of the order (h_2/d) smaller than the osmotically induced flow velocities in the extracellular channel. The cell interior can thus be treated as a constant pressure and concentration reservoir or a homogeneous compartment. The very small water and solute fluxes that occur inside the cell could be determined from a higher order theory in which terms of order h_2/d are retained in the boundary conditions for the governing equations in the cell interior. The lowest order solutions for these intracellular fluxes involve the solution of a two- or three-dimensional Laplace equation for the solute concentration and similarly a multidimensional Stokes slow flow equation for the water streamlines. The cell interior can not be treated by quasi one-dimensional theory as is done for the channel since the fluxes within the cell are not unidirectional. In fact, we shall show that a closed streamline recirculation pattern is established in the corneal endothelium. These important differences between the governing equations for the channel and cell interior are neglected in the recent quasi one-dimensional model presented in references 20 and 21.

The solution to Eqs. 1–5 must satisfy the boundary conditions

$$C(0) = \Gamma_1 \tag{7a}$$

$$C(L_1 + L_2) = \Gamma_2 \tag{7b}$$

$$P(L_1 + L_2) - P(0) = \Delta p \text{ (hydrostatic)} + \sigma_{TJ} RT [\Gamma_1 - C(L_1)] + RTZ_1 \tag{7c}$$

where Δp (hydrostatic) is the hydrostatic pressure difference imposed across the cell layer and the osmotic force exerted by the solute concentration difference across the tight junction has been replaced by its equivalent pressure difference. Boundary conditions 7a and b are an approximation that neglect unstirred layers on the cell faces and the diffusional mixing that occurs at the channel exits. As shown in Goldgraben and Weinbaum (24) this diffusional relaxation occurs on a length scale of the order of five channel heights. A more correct boundary condition, as discussed in Sackin and Boulpaep (11), is to treat the channel inflow or outflow as part of an unstirred layer of prescribed thickness. This problem has been studied in detail by Pedley and Fischbarg[1,2] who found that the corrections due to these unstirred layers do not exceed 15%. These small corrections have been neglected in the present model because of the additional mathematical complexity they would introduce. Boundary condition (Eq. 7b) is valid in the limit where the diffusion at resistance of the unstirred layer is small compared with the channel. These conditions are usually satisfied in long narrow channels that are widely separated provided that the unstirred layer thickness is not large compared with the channel spacing, see Kelles and Stein (25).

The solute concentration and solute and water fluxes must also be continuous at $x = L_1$ where the tight junction opens into the extracellular channel. This requires that at $x = L_1$

[1]Pedley, T. J., and J. Fischbarg. 1980. Unstirred layer effects in osmotic water flow across gallbladder epithelium. *J. Memb. Biol.* 5:89–102.

[2]Pedley, T. J. 1981. The interaction between stirring and osmosis. *J. Fluid Mech.* In press.

$$C(L_1^-) = C(L_1^+) \tag{8a}$$

$$\left(-Dh_1 \frac{dC(x)}{dx} + h_1 V(x) C(x)\right)_{x=L_1^-} = \left(-Dh_2 \frac{dC(x)}{dx} + h_2 V(x) C(x)\right)_{x=L_1^+} \tag{8b}$$

$$h_1 V(L_1^-) = h_2 V(L_1^+). \tag{8c}$$

The solution of the boundary value problem defined by Eqs. 1–5 and boundary conditions (Eqs. 7 and 8) is considerably more difficult than previous microscopic models which considered only the extracellular channel. These previous models satisifed only Eqs. 1–3. Thus the extracellular concentration was uncoupled from the intracellular solute and protein concentrations which were arbitrarily fixed. In the present model Eqs. 4 and 5 can be thought of as integral side conditions on these concentrations which must be satisfied simultaneously with the channel-flow equations. Fortunately, A_c and C_c are unknown constants rather than unknown functions so that the integrals in Eqs. 4 and 5 can be evaluated analytically if closed form approximate expressions for $C(x)$ can first be obtained in terms of A_c and C_c. The other difficulty is that the channel-flow equations are nonlinear. However, as first shown by Segel (26), when Eqs. 1–3 are written in dimensionless form a critical dimensionless parameter $\nu = \alpha/P_w\Gamma_0$ appears. For $\nu \ll 1$ all the variables can be expressed as a perturbation series expansion in ν and the problem reduced to an ordered array of linear equations. The nontrivial extension of Segel's approach to include the simultaneous solution of Eqs. 4 and 5 is presented in the Appendix. A typical value of ν for corneal endothelium is 0.026. One finds that for this value of ν truncating the series after the first two terms introduces errors of <4% in the channel fluxes.

THE CORNEAL ENDOTHELIUM

To illustrate how the general model developed in the previous section can be applied to a particular epithelium, we shall examine in detail the transport function of the corneal endothelium in vitro and in vivo.

The cornea (27, 28) separates the aqueous humor of the anterior chamber of the eye from the tears and the external world (Fig. 2). The stroma, roughly 90% of the corneal thickness, contains an organized regular array of collagen fibrils whose order is maintained by the mutual repulsive forces between the fibers. Such repulsive forces cause the stroma to swell absorbing water from the surrounding media. (An alternative theory [29] proposes that this swelling pressure is due to the osmotic force caused by ions held by the electrically charged groups on the collagen fibrils.) This swelling pressure sucking fluid into the stroma is about 60 Torr (30–32). When the stroma is swollen the distance between the fibers is increased, their mutually repulsive forces are reduced, and the swelling pressure decreased. Moreover, in the water-swollen cornea, with the reduction of these interactive forces, the spatial regularity required for corneal transparency is lost. It is believed that the passive water flux into the stroma generated by the stromal swelling pressure is counteracted through local osmosis produced by ion pumps strategically located in the endothelium (33–36).

The corneal endothelium (28, 37–41) is a single layer of cells. A diagonal across their roughly hexagonal faces is about four times as long as the cell layer height. The extracellular channel between adjacent cells is ~200–300 Å wide. It is quite tortuous so that its total length

may be as much as twice the cell layer height. The aqueous end of this channel is "sealed" by a "tight" junctional complex. The high water and salt permeabilities of this tissue, low electrical resistance (<100 Ω-cm^2) and small potential difference (0.5 mV) (42–50) and the fact that large molecular markers such as horseradish peroxidase penetrate these junctions (51, 52) demonstrates that these tight junctions are actually rather leaky. Since water is moved by the fluid pump from the stromal side toward the tight junctions on the aqueous face, this tissue is an example of what Diamond and Bossert (14) call a "backwards" fluid transporting epithelia. (In a "forward" transporting tissue water flows away from the tight junctions.) In our work, Fig. 3, we have adopted the ultrastructural dimensions used by Fischbarg (36), which are within the ranges suggested by other studies.

The working of the endothelial pump has been elegantly demonstrated by measuring its ability in vitro to transport 2–6 μl/h/cm^2 of water between bathing solutions of equal tonicity (34–36). A hydrostatic pressure of 60–105 Torr (36, 53) counter to the direction of flow is required to stop the pump. To help understand how water and salt flow through the endothelium, a great deal of effort has gone into measuring its water and salt permeabilities and the strength of the bicarbonate pump, which might be the ion responsible for driving the water flow.

As in other epithelia, the two types of models described in the Introduction have been proposed to explain the working of the fluid pump in the corneal endothelium. Shapiro and Candia (54) and Rehm and Spangler (55, 56) used thermodynamic models to calculate the flows of solute and water between the three compartments formed by the stroma, the endothelial cells, and the aqueous humor. In both models the extracellular channels are transcellular shunts whose similar ends connect the stroma with the aqueous chamber. Lim and Fischbarg (37, 57) investigated the other type of model, the microscopic model. They used a perturbation analysis to solve analytically for the water flow driven by a standing gradient of salt in the extracellular channel. As is usual in such channel models they did not consider the transcellular flows of solute and water. The endothelium has also been treated in less detail, where the whole cell layer is regarded as a single membrane in the models developed to follow water flow through the entire cornea by Friedman (58–61) and Klyce and

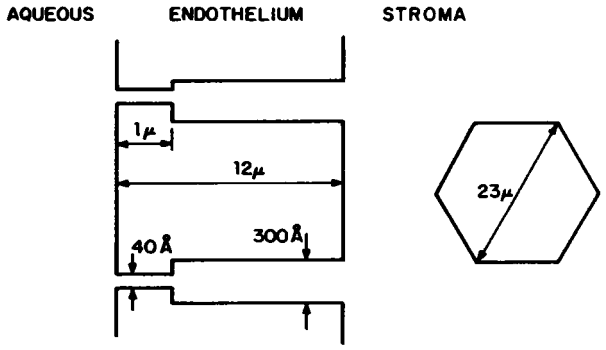

FIGURE 3 Transverse and face-on views showing the ultrastructural dimensions used to model the corneal endothelium. The tortuous extracellular channel appears straightened out in this idealized picture.

Russel (62). As described in the Introduction neither these thermodynamic nor microscopic models of the corneal endothelium can provide a complete understanding of the interaction between the component cells and the three different environments that each cell must encounter as one proceeds along its plasmalemma from the stromal, to the lateral, to the aqueous margins.

RESULTS

The values of the parameters used in the model are given in Table I. Since the cell layer has flat cells with hexagonal faces, the apical and basal areas and cell perimeter are given by $S_1 = S_2 = 3\sqrt{3}\, d^2/8$ and $\ell = 3d$. For the dimensions of the extracellular channel and tight junction we adopt the values given by Fischbarg (36). We assume a typical concentration of 300 mosmol/liter for the apical and basal bathing solutions at a temperature of 37°C. The diffusion coefficient for ions within the channel is unknown so we chose $D = 10^{-5}$ cm^2/s, similar to the value adopted by other workers (13–14, 16, 21, 26, 57) and slightly less than the free solution value for NaCl. Because the corneal endothelium is so leaky we expect that the reflection coefficient across the tight junctions, σ_{TJ}, to be very small. Since σ_{TJ} cannot be measured directly it must be estimated from the available theories (72–75) which predict that for small ions in a narrow slit, the reflection coefficient should be between 0.03 and 0.20. For simplicity we set $\sigma_{TJ} = 0$ which introduces an error of <12% in the calculated net fluid flow even if σ_{TJ} is 0.10.

Because the relative solute and water permeabilities of the aqueous, lateral, and stromal portions of the cell membrane of the corneal endothelium are not accurately known we adopt the simplest assumption; namely, that these permeabilities are constant around the cell border. In fact, restricting ourselves to the fewest number of input parameters places unnecessarily harsh constraints on our model. For example, if we set the aqeous cell membrane water permeable (P_{w1}) much greater than that of the stromal cell membrane (P_{w2}), we increase the net water flow. Similarly, if the solute permeability of the lateral cell membrane (P_s) is much larger than that of the aqueous cell membrane (P_{s1}), the passive leak of solute from the channel into the cell replaces the requirement for solute pumps on the lateral cell membrane. We prefer, however, to test the simplest hypothesis for cell membrane permeability and in this manner avoid the prolification of unknown parameters.

The water permeability measured for the membranes of different cells ranges from 0.00069 to 0.64 cm^4/mol/s (2,76). To match the experimentally determined fluid transport rate required that we set $P_w = P_{w1} = P_{w2} = 0.275$ cm^4/mol/s. Although the value of P_w for the corneal endothelial cells is unknown, our assumed value seems reasonable because it does not exceed the highest $P_w = 0.64$ cm^4/mol/s reported for cat erythrocytes (77) and it is close to the $P_w = 0.23$ cm^4/mol/s reported both for frog muscle cells (78) and recently for rabbit corneal epithelial cells (79). The net fluid flow calculated from our model is not very sensitive to the assumed value of P_w. For example, the net fluid flow approximately doubles (from 2.5 to 5.7 μl/h/cm^2) as P_w is increased by a factor of 10 (from 0.257 to 2.57 cm^4/mol/s). This is because as P_w is raised the fluid flow increases the amount of solute swept into the extracellular channel which reduces the concentration differences driving the osmotically induced flow.

TABLE I
INPUT PARAMETERS FOR OUR MODEL OF THE CORNEAL ENDOTHELIUM

	Geometry		
d	cell face diagonal	23 μm*	2.3×10^{-3} cm*
h_1	width of tight junction	40 Å	4.0×10^{-7} cm
L_1	length of tight junction	1 μm	1.0×10^{-4} cm
h_2	width of extracellular channel	300 Å	3.0×10^{-6} cm
L_2	length of extracellular channel	12 μm	1.2×10^{-3} cm
	Boundary conditions		
Γ_1	aqueous (apical) solute concentration	300 mosmol/liter	3.0×10^{-4} M/cm^3
Z_1	aqueous (apical) impermeant solute concentration	0	0.0
Γ_2	stromal (basal) solute concentration	300 mosmol/liter	3.0×10^{-4} M/cm^3
Δp	(hydrostatic) in vitro	0	0.0
	in vivo	−70 Torr	-9.33×10^4 dyne/cm^2
	Constants		
T	temperature	37° C	310.0° K
μ	absolute viscosity of water		7.0×10^{-2} dyne-s/cm^2
D	solute diffusion coefficient		1.0×10^{-5} cm^2/s
σ_{TJ}	solute reflection coefficient at tight junctions		0.0
	Cell membrane		
P_s	lateral solute poermeability		3.0×10^{-7} cm/s
P_{s1}	aqueous (apical) solute permeability		3.0×10^{-7} cm/s
P_{s2}	stromal (basal) solute permeability		3.0×10^{-7} cm/s
P_w	lateral water permeability		0.257 cm^4/M/s
P_{w1}	aqueous (apical) water permeability		0.257 cm^4/M/s
P_{w2}	stromal (basal) water permeability		0.257 cm^4/M/s
α	later solute pump strength		2.0×10^{-6} cm/s
α_1	aqueous (apical) solute pump strength		4.4×10^{-6} cm/s
α_2	stromal (basal) solute pump strength		0.0
	Unknowns determined by the above parameters		
C_c	intracelular solute concentration	295.2 mosmol/liter	2.952×10^{-4} M/cm^3
A_c	intracellular protein concentration	1.9 mosmol/liter	1.9×10^{-6} M/cm^3
$C(x)$	extracellular channel solute concentration	(Figs. 5, 7)	M/cm^3
$P(x)$	extracellular channel hydrostatic pressure	(Figs. 5, 7)	dyne/cm^2
$V(x)$	extracellular channel fluid velocity	(Figs. 5, 7)	cm/sec

*Penultimate column gives values in the most familiar units and the last column gives the values in c.g.s. units used in the model.

Cell membranes display a large range of solute permeabilities from 10^{-8} to 10^{-5} cm/s (76, 80) of which we chose the geometric mean $P_s = P_{s1} = P_{s2} = 3 \times 10^{-7}$ cm/s. Since we assume that more solute is moved across the cell membrane by active pumps rather than by passive leaks, our results are not sensitive to the value of P_s as long as it remains less than the solute pump strength α.

Markers to a ouabain-inhibitable ATPase have been found to bind exclusively to the lateral cell membrane along the extracellular channel (81–83). The calculated net fluid transport rate is approximately proportional to the lateral membrane solute pump strength α, and we chose $\alpha = 2.0 \times 10^{-6}$ cm/s to be consistent with the experimentally determined fluid transport rate. Since there is no experimental information on solute pumps in the rest of the cell membrane as explained below, we investigated the sensitivity of the model to various pump location possibilities. In the model given in Table I, we chose the stromal solute pump strength $\alpha_2 = 0$. As explained in the Appendix, establishing α and α_2 determines the aqueous solute pump strength $\alpha_1 = 4.4 \times 10^{-6}$ cm/s through the compatibility condition that the amount of solute entering the cell equal the amount of solute leaving the cell.

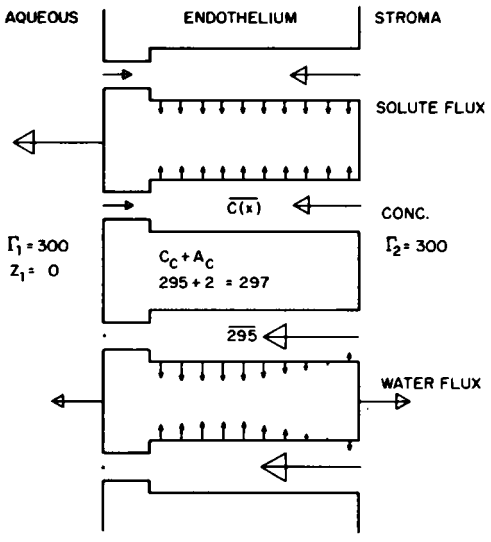

FIGURE 4

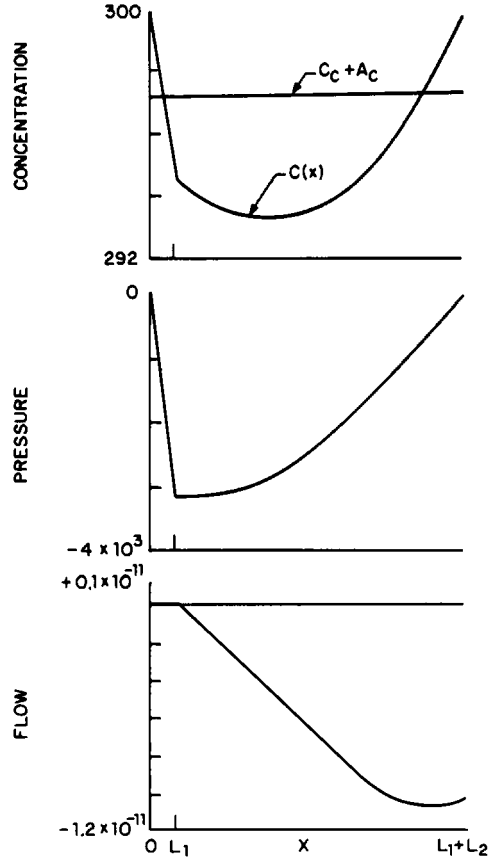

FIGURE 5

FIGURE 4 Flows of solute and the water across the corenal endothelium. Depicted is the case where the stroma is swollen, such as when an isolated cornea with its epithelium scraped off is placed in a chamber between identical bathing solutions. There is a net flow of water from the stroma into the aqueous. Under the bar is denoted the average concentration (mosmol/liter) within the extracellular channel.

FIGURE 5 Variation of solute concentration (mosmol/liter), hydrostatic pressure (dyne/cm^2), and volume flow (cm^2/s/cell) along the extracellular channel for the model shown in Fig. 4. The aqueous is at $X = 0$ and the stroma at $X = L_1 + L_2$.

Figs. 4 and 5 show the results of the calculation when the stromal swelling pressure Δp (hydrostatic) = 0. This model is meant to duplicate the in vitro water flux measurements by Maurice (34) and Fischbarg et al. (35, 36). As can be seen by summing the water flux vectors at either the aqueous or stromal tissue margins there is a net flow of water from the stroma towards the aqueous which equals 2.5 μl/h/cm^2. To predict the in vivo conditions, in Figs. 6 and 7, a large enough stromal swelling pressure gradient Δp (hydrostatic) = -70 Torr has been imposed so that there is no net water flow.

Given all the above input parameters, the model predicts the intracellular and extracellular channel concentrations and the fluid velocity at any position along the channel. As shown in the Appendix, we used these results to evaluate the concentration differences and velocities that drive solute and water flows across the aqueous and stromal cell faces and the aqueous and stromal ends of the extracellular channel. This made it possible to calculate the net solute (J_s) and water (J_v) flows across the cell layer. These net flows are a function of the assumed

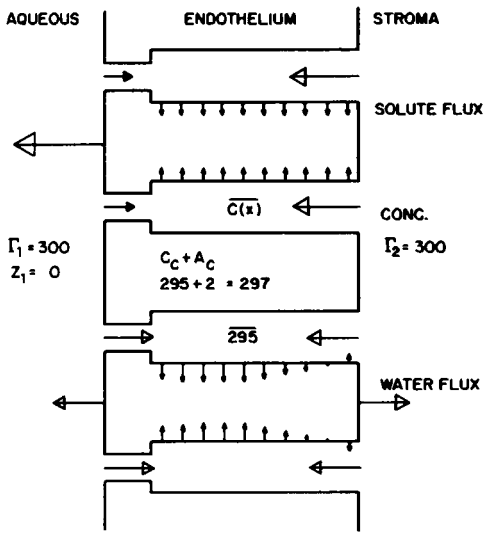

FIGURE 6

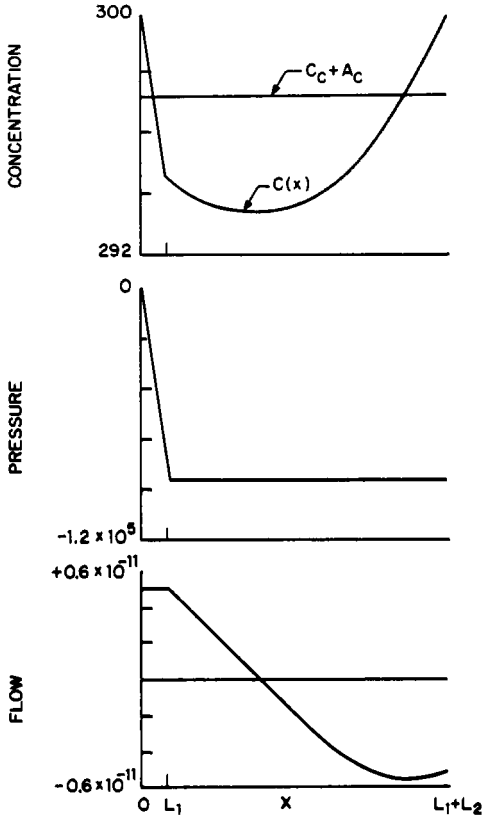

FIGURE 7

FIGURE 6 In vivo there is a stromal swelling pressure not shown in Fig. 3. Here we have imposed a pressure Δp (hydrostatic) = -70 Torr which forces enough water through the tight junctions towards the stroma so that there is no net water flow.

FIGURE 7 Variation of solute concentration (mosmol/liter), hydrostatic pressure (dyne/cm^2), and volume flow (cm^3/s/cell) along the extracellular channel for the model shown in Fig. 5.

boundary concentrations Γ_1 and Γ_2 of mobile solute in the aqueous and stromal bathing solutions and the concentration of the solute Z_1 impermeant to the cell layer in the aqueous bath. Thus we calculated the net flows $J_s(\Gamma_1, \Gamma_2, Z_1)$ and $J_v(\Gamma_1, \Gamma_2, Z_1)$ for various values of Γ_1, Γ_2, and Z_2. We found that the changes in the net flows were approximately linear with small changes (e.g., 10 mosmol/liter) in $\Gamma_2 - \Gamma_1 = \Delta C$ and $Z_1 = \Delta Z$. We can therefore determine the net transendothelial permabilities using the definitions that the hydraulic conductivity $L_p = [J_v(\Gamma_1, \Gamma_1, \Delta Z) - J_v(\Gamma_1, \Gamma_1, 0)]/RT\,\Delta Z$, and the solute permeability $P_s = [J_s(\Gamma_1 + \Delta C, \Gamma_1, 0) - J_s(\Gamma_1, \Gamma_1, 0)]/\Delta C$. The reflection coefficient across the cell layer σ is equal to the fluid flow induced by a concentration difference ΔC divided by the fluid flow induced by an equal concentration difference ΔZ of the solute impermeant to the cell layer. Therefore, we determined the net reflection coefficient by $\sigma = [J_v(\Gamma_1 + \Delta C, \Gamma_1, 0) - J_v(\Gamma_1, \Gamma_1, 0)]/[J_v(\Gamma_1, \Gamma_1, \Delta Z) - J_v(\Gamma_1, \Gamma_1, 0)]$. Note that the net reflection coefficient σ depends on the calculated net water flows and thus it is a complex nonlinear function of the input parameters, but it is approximately equal to the average of the reflection coefficients through the aqueous cell face and the tight junction weighted by their respective water permeabilities. Since both pathways have roughly the same water permeability but σ (cell membrane) ~ 1 and σ (tight junction) ~ 0, the net $\sigma \sim \frac{1}{2}$. The values that we calculate for the hydraulic conductivity, solute permeability, and reflection coefficient compare favorably with the measured values (Table II).

Because there are no large concentration gradients within the cell, and if the external solutions are voluminous enough so that their concentration is not significantly affected by the solute pumps of the cell, then pumping solute out of the cell through the aqueous cell face produces the same concentrations within the cell and the extracellular channel, and thus the same water flows, as pumping that same amount of solute out of the cell through its stromal cell face. However, the location of the solute pumps determines the net solute flow across the cell layer as seen in Fig. 8. The location of the ion pumps and the species of ions pumped across each portion of the cell membrane of the corneal endothelium is not known. Inasmuch as the net active bicarbonate flux has been implicated in water movement, we compare in Table II these measurements in the corneal endothelium with the solute fluxes predicted by the three alternative solute pump locations shown in Fig. 8. (Note that the simplistic adage that "water follows salt" is not always true. Water flows are not driven by solute flows but by solute concentration differences which are determined by the interaction of the solute flow with the tissue geometry. For example, in Fig. 8*c*, the net flow of water is towards the aqueous while the net flow of solute is in the opposite direction, towards the stroma.)

Because our model can be used to determine the net solute and water flows, we can calculate the concentration of the transported fluid. Since, as described above, the net amount of solute transported depends on the location of the solute pumps, which are unknown, we cannot predict with certainty the concentration of this fluid. However, if there are solute pumps located on the aqueous, but not the stromal cell faces (Fig. 8*a*) or equally on both aqueous and stromal cell faces (Fig. 8*b*), then the predicted concentration of the transported fluid is hypertonic; namely, 1,557 and 610 mosmol/liter, respectively. On the other hand, if there are solute pumps on the stromal but not the aqueous cell face (Fig. 8*c*) then the net solute flow is towards the stroma, opposite in direction to the hypotonic net fluid transport. It should be noted that the complicated and incompletely understood nature of the unstirred

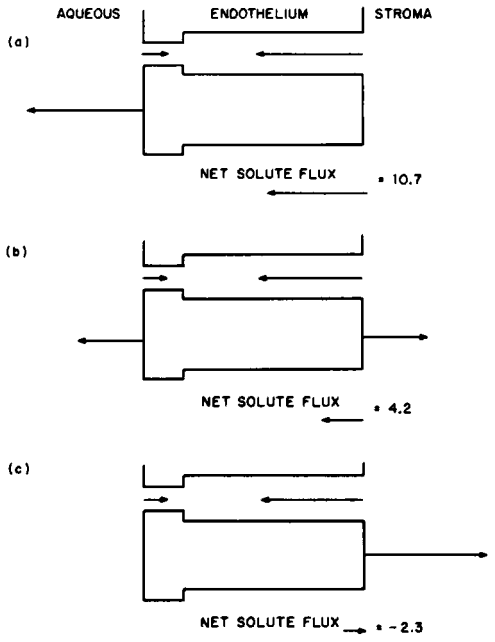

FIGURE 8 Shown are the cellular and paracellular solute fluxes when in addition to the solute flux across the lateral cell membrane there are, (*a*) solute pumps exclusively on the aqueous cell face, (*b*) equal solute pumps on both the aqueous and stromal cell faces, and (*c*) solute pumps exclusively on the stromal cell face. In each case the net solute flux in 10^{-10} mol/s/cm^2 is indicated.

layers contiguous to the cell layer and the mixing with these layers of the flows exiting the extracellular channel may have a significant influence on the concentration of the transported fluid. At this stage of development, however, our model does not address itself to such issues.

DISCUSSION

Water Transport in Vitro

The seemingly complex solution given in the Appendix for Eqs. 1–5 can be understood in simple qualitative terms. We emphasize the importance of the water conservation equation that the flow of water into the cell equals the flow of water out of the cell, which is equivalently stated in Eq. 6 that the total intracellular concentration equals the average of the environmental concentrations surrounding the cell weighted by the product of the cell membrane water permeability and area facing each concentration.

Concentration differences are required to drive water flows osmotically. The cell must therefore differ in concentration from its surrounding solutions. (This must be true whether water flows through either transcellular or paracellular routes. Even if a standing osmotic gradient drives the water flow entirely through the extracellular channel the water that flows through the channel came from the cell and so must be replenished into the cell from the outside; such an osmotic flow could only be driven by concentration differences between the cell and its bathing solutions.) Because the intracellular concentration is simply the average of the concentrations surrounding the cell, at least one of those concentrations must differ from

the others for water flow to occur. The cell creates this concentration difference through the action of the solute pumps on its cell membrane. It is difficult for these pumps to alter the concentration in an extended solution, such as that facing the apical or basal cell membrane (except if the epithelia surrounds a small lumen as in the case of the kidney proximal tubule [18, 19]). However, these solute pumps can significantly alter the concentration within the small-volume extracellular channel. In our view, the importance of the channel is not the magnitude of the standing gradient but that its average concentration differs from that of the apical and basal solutions. In the backwards fluid transporting corneal endothelium, we calculate the channel's average concentration to be 295 mosmol/liter compared with the 300 mosmol/liter solution facing the aqueous and stromal borders of the cell. Since 55% of the surface of the cell borders the channel, if the cell membrane has the same water permeability on all sides, the total intracellular concentration is $0.55 \times 295 + 0.45 \times 300 = 297$ mosmol/liter. Note that by the definition of an average, the total intracellular concentration must be higher than that of the channel while at the same time being lower than that of the aqueous and stromal solutions. Also note the importance of including the intracellular protein concentration so that the water conservation Eq. 6 can be satisfied.

Since the 297 mosmol/liter cell is hypotonic to the 300 mosmol/liter aqueous and stromal bathing solutions, water will flow equally across both cell faces from the cell into the aqueous and the stroma. (The back leak of water across the stromal cell membrane counter to the direction of the net water flow is proportional to the stromal [basal] cell membrane water permeability P_{w2}. Some previous models [11, 12, 20] eliminated it by enforcing the rather stringent condition that $P_{w2} = 0$.) The water that flows out of the cell is replaced by water driven into the cell from the extracellular channel which at an average of 295 mosmol/liter is hypotonic with respect to the 297-mosmol/liter cell.

When water from the extracellular channel is sucked into the cell the hydrostatic pressure within the channel falls so that there is a suction, as seen in Fig. 5, forcing water into the channel to replace the water that flowed into the cell. New water can flow into the channel from either the tight-junction aqueous side through an entrance slit 40 Å wide or from the stromal side through an entrance slit 300 Å wide. Most of the water flows into the channel from the lower resistance stromal side. (Even though the channel is hypotonic to the aqueous and stroma there will be no significant osmotic force at the channel exits if the exits are sufficiently wide and molecular level forces sufficiently weak so as not to impede the passage of small ions. In the corneal endothelium which has particularly leaky tight junctions, these conditions are probably met.)

Thus, there is a net flow of water across the endothelium even though water leaves the cell in equal amounts in opposite directions at both the aqueous and stromal faces because most of the water that entered the cell through the extracellular channel came from the stroma. There is a net flow of water because of the geometric asymmetry of the extracellular channel—one end is effectively closed by the large hydraulic resistance of the tight junction (although its dimensions are large compared with the water and ions that pass through it) while the other end is open.

Water Transport In Vivo

The in vitro behavior just described is that observed in water flux experiments where the stroma is swollen and the stromal swelling pressure negligible. Now we examine the situation

in the living eye, Figs. 6 and 7, where the stroma is not swollen and a finite stromal swelling pressure exists. As before, because the cell is hypotonic, osmotic forces drive equal amounts of water in opposite directions through the aqueous and stromal cell faces. However, unlike the in vitro situation, the additional pressure gradient is now due to the stromal swelling pressure and the intraocular pressure forces water through the tight junctions from the aqueous into the extracellular channel. The amount of water entering the extracellular channel from the aqueous side through the tight junctions is equal to the amount of water entering the channel from the stromal side. Thus, there is no net water flow across the cell layer. There is, however, a recirculation of water. Equal amounts of water first enter the extracellular channel from opposite ends of the channel. This water must then cross the lateral membrane of the cell to satisfy continuity and finally equal amounts of water must exit the cell in opposite directions through the aqueous and stromal cell faces if the bathing solutions are isotonic. The "leak" of water across the endothelium into the stroma driven by the difference between the stromal swelling pressure and the intraocular pressure has been balanced by the action of the endothelial "pump."

What if the leak/pump balance is disturbed; for example, if an excess of water is forced into the stroma causing it to swell. Since the stromal swelling pressure varies inversely with the stromal hydration, the pressure gradient across the endothelium will be lowered, less water will be forced through the tight junctions, and there will be a net flow of water out of the stroma into the aqueous until the stroma is unswollen. Thus, there is a self-adjusting homeostatic mechanism already contained within our model to maintain the stroma at sufficient dehydration for corneal transparency.

We believe that one of the strong points of our model is that it provides a natural explanation for the "leakiness" of the corneal endothelium. At first, one might think that such a leaky limiting barrier is unwisely inefficient. However, we have seen the tight junctions are just leaky enough so that at physiological stromal swelling pressures, the leak is matched by the pump. Thus, we evoke the teleological fallacy to argue that the width of the tight junctions is not arbitrary, but is directly related to the normal stromal swelling pressure. Moreover, it is the leakiness that allows for the existence of the homeostatic mechanism described above. We also speculate that the existence of a circulation of water, with no net flow in the balanced physiological state, rather than being wasteful, might be a way to assist the flow of nutrients into and wastes out of an avascular cornea.

SUMMARY

We have solved the equations that model the flows of solute and water through the cells and extracellular channels of an epithelial tissue. An important feature of our model is that we require that amount of solute and water entering the cell must equal the amount of solute and water leaving the cell. This allows us to couple the intracellular state with the extracellular environment.

From the conservation of water flux through any cell we showed that for a cell surrounded by environments of different concentrations, the total intracellular concentration is equal to the average of the concentrations surrounding the cell weighted by the product of the cell-membrane water permeability and surface area facing each concentration.

TABLE II
MEASUREMENTS VS. MODEL CALCULATIONS

Measurement	(Reference)	Theory	
Hydraulic conductivity L_p (10^{-12} cm^3/s/dyne)			
1.4	(63)		
3.0	(64)		
3.0*	(35, 36)		
12.0‡	(35, 22)	14.2	
13.0	(65)		
15.0	(66)		
42.0	(62)		
Salt Permeability P_s (10^{-5} cm/sec)			
2.0	(63)		
2.0	(67)		
2.1	(68)	1.6	
2.2	(69)		
8.0	(62)		
Salt reflection coefficient (σ)			
0.4	(63)		
0.45	(62)	0.42	
0.6	(66)		
Net active bicarbonate flux (10^{-10} mol/s/cm^2)			
2.9	(50)	10.7	(8a)§
4.7	(62)	4.2	(8b)
4.7	(70, 71)	−2.3	(8c)

* Fluid flow towards stroma.
‡ Fluid flow towards aqueous.
§ Shown in Fig. 8 a–c.

We applied this general model to calculate the flows of solute and water expected to exist in the corneal endothelium under different conditions. We found, as seen in Fig. 4, that when the stroma swells in the bath, the cell at 297 mosmol/liter is slightly hypotonic with respect to the 300 mosmol/liter bathing solutions. This drives water out both the aqueous and stromal cell faces. This water is replaced from the extracellular channel. There is a net flow of water because more water enters the channel through the open stromal end of the channel than through the higher resistance tight junction. In vivo, when there is a stromal swelling pressure, as shown in Fig. 6, there is a recirculation of water at both the basal and stromal borders of the cell but no net flow of water. We described how this leads to a homeostatic control mechanism for maintaining the proper level of stromal hydration.

Our model is in reasonable agreement with the reported values of the hydraulic conductivity, salt permeability, salt reflection coefficient, and net active ion pump rate of the corneal endothelium as shown in Table II.

APPENDIX

We must solve Eqs. 1–5 subject to boundary and match conditions Eqs. 7–8 and to find C_c^*, A_c^*, $C^{I*}(X^*)$, $C^{II*}(X^*)$, $V^{I*}(X^*)$, $V^{II*}(X^*)$, $P^{I*}(X^*)$, and $P^{II*}(X^*)$ where the stars denote dimensional variables and the superscript I labels the tight junctional region $0 \leq X^* \leq L_I$ and II the rest of the

extracellular channel $L_1 \le X^* \le L_1 + L_2$. We can define the dimensionless lengths, concentrations and velocities as $X^{\mathrm{I}} = X^*/L_1$, $X^{\mathrm{II}} = (X^* - L_1)/L_2$, $\Gamma_0 = (\Gamma_1^* + \Gamma_2^*)/2$, $C_c = C_c^*/\Gamma_0$, $A_c = A_c^*/\Gamma_0$, $C^{\mathrm{I}}(X^{\mathrm{I}}) = C^{\mathrm{I}*}(X^*)/\Gamma_0$, $C^{\mathrm{II}}(X^{\mathrm{II}}) = C^{\mathrm{II}*}(X^*)/\Gamma_0$, $V^{\mathrm{I}}(X^{\mathrm{I}}) = V^{\mathrm{I}*}(X^*)/(2\alpha L_1/h_1)$, and $V^{\mathrm{II}}(X^{\mathrm{II}}) = V^{\mathrm{II}*}(X^*)/(2\alpha L_2/h_2)$.

We expand the unknowns as a power series in the small parameter $\nu = \alpha/(P_w\Gamma_0)$:

$$
\begin{aligned}
C_c &= C_{c0} + \nu C_{c1} + \nu^2 C_{c2} + \cdots \\
A_c &= A_{c0} + \nu A_{c1} + \nu^2 A_{c2} + \cdots \\
C^{\mathrm{I}}(X^{\mathrm{I}}) &= C_0^{\mathrm{I}}(X^{\mathrm{I}}) + \nu C_1^{\mathrm{I}}(X^{\mathrm{I}}) + \nu^2 C_2^{\mathrm{I}}(X^{\mathrm{I}}) + \cdots \\
C^{\mathrm{II}}(X^{\mathrm{II}}) &= C_0^{\mathrm{II}}(X^{\mathrm{II}}) + \nu C_1^{\mathrm{II}}(X^{\mathrm{II}}) + \nu^2 C_2^{\mathrm{II}}(X^{\mathrm{II}}) + \cdots \\
V^{\mathrm{I}}(X^{\mathrm{I}}) &= V_0^{\mathrm{I}}(X^{\mathrm{I}}) + \nu V_1^{\mathrm{I}}(X^{\mathrm{I}}) + \nu^2 V_2^{\mathrm{I}}(X^{\mathrm{I}}) + \cdots \\
V^{\mathrm{II}}(X^{\mathrm{II}}) &= V_0^{\mathrm{II}}(X^{\mathrm{II}}) + \nu V_1^{\mathrm{II}}(X^{\mathrm{II}}) + \nu^2 V_2^{\mathrm{II}}(X^{\mathrm{II}}) + \cdots
\end{aligned}
\tag{A1}
$$

In the case of the corneal endothelium $\nu = 0.026$. The pressure is not included in these equations because it is determined from the velocity through Eq. 3. To determine the unknown coefficients and functions we use these expansions to evaluate the extracellular channel transport Eqs. 1 and 2, the cell conservation integrals Eqs. 4 and 5, and the boundary and matching condition Eqs. and 7 and 8. We can now equate the coefficients of equal powers of ν using the fact noted by Segel (24) that terms with the factors $\eta_1 = Dh_1/(2\alpha L_1^2)$ and $\eta_2 = Dh_2/(2\alpha L_2^2)$ are much greater than unity and so should be treated as order $(1/\nu)$. For the cornea endothelium $\eta_1 = 100.0$ and $\eta_2 = 6.2$. Because the protein concentration is much less than the mobile solute concentration we set $A_{c0} = 0$. Thus, to zeroth order in we find that Eqs. 1a, b, 4, 5, 7a, b, 8a, b) become

$$
\begin{aligned}
-\eta_1 \mathrm{d}^2 C_0^{\mathrm{I}}(X^{\mathrm{I}})/(\mathrm{d}X^{\mathrm{I}})^2 &= 0 \\
-\eta_2 \mathrm{d}^2 C_0^{\mathrm{II}}(X^{\mathrm{II}})/(\mathrm{d}X^{\mathrm{II}})^2 &= 0 \\
(\sqrt{3}d/8L_2)[C_{c0}(\alpha_1 + \alpha_2 + P_{s1} + P_{s2}) - (P_{s1} + P_{s2})] & \\
+ P_s C_{c0} - (P_s + \alpha)\int_0^1 C_0^{\mathrm{II}}(X^{\mathrm{II}})\mathrm{d}X^{\mathrm{II}} &= 0 \\
(\sqrt{3}d/8L_2)[P_{w1}(1 - C_{c0}) + P_{w2}(1 - C_{c0})] - P_w C_{c0} & \\
+ P_w \int_0^1 C_0^{\mathrm{II}}(X^{\mathrm{II}})\mathrm{d}X^{\mathrm{II}} &= 0
\end{aligned}
$$

$$
\begin{aligned}
C_0^{\mathrm{I}}(0) &= 1 \\
C_0^{\mathrm{II}}(1) &= 1 \\
C_0^{\mathrm{I}}(1) &= C_0^{\mathrm{II}}(0) \\
-\eta_1 L_1 \mathrm{d}C_0^{\mathrm{I}}(X^{\mathrm{I}})/\mathrm{d}X^{\mathrm{I}} &= -\eta_2 L_2 \mathrm{d}C_0^{\mathrm{II}}(X^{\mathrm{II}})/\mathrm{d}X^{\mathrm{II}},
\end{aligned}
\tag{A2}
$$

while Eqs. 2a, b, 7c, 8c) reduce to $0 = 0$. The coefficients of the zeroth order solution that satisfy Eqs. A2 are found to be $C_{c0} = C_0^{\mathrm{I}}(X^{\mathrm{I}}) = C_0^{\mathrm{II}}(X^{\mathrm{II}}) = 1$ with the compatibility condition that $\alpha_1 + \alpha_2 = 8\alpha L_2/(\sqrt{3}d)$.

To find the first order coefficients in the expansion A1 we now evaluate the first order terms in ν to find:

$$
-\eta_1 \nu \mathrm{d}^2 C_1^{\mathrm{I}}(X^{\mathrm{I}})/(\mathrm{d}X^{\mathrm{I}})^2 + \mathrm{d}V_0^{\mathrm{I}}(X^{\mathrm{I}})/\mathrm{d}X^{\mathrm{I}} = 0 \tag{A3a}
$$

$$
-\mathrm{d}^2 C_1^{\mathrm{II}}(X^{\mathrm{II}})/(\mathrm{d}X^{\mathrm{II}})^2 + K^2 \mathrm{d}V_0^{\mathrm{II}}(X^{\mathrm{II}})/\mathrm{d}X^{\mathrm{II}} = -K^2 \tag{A3b}
$$

$$
\mathrm{d}V_0^{\mathrm{I}}(X^{\mathrm{I}})/\mathrm{d}X^{\mathrm{I}} = 0 \tag{A3c}
$$

$$dV_0^{II}(X^{II})/dX^{II} = C_1^{II}(X^{II}) - C_{c1} - A_{c1} \tag{A3d}$$

$$(\sqrt{3}d/8L_2)[(\alpha_1 + \alpha_2 + P_{s1} + P_{s2})C_{c1} - P_{s1}\gamma_1 - P_{s2}\gamma_2] + P_sC_{c1} - (P_s + \alpha)\int_0^1 C_1^{II}(X^{II})dX^{II} = 0 \tag{A3e}$$

$$(\sqrt{3}d/8L_2)[P_{w1}(\gamma_1 + \gamma_z - C_{c1} - A_{c1}) + P_{w2}(\gamma_2 - C_{c1} - A_{c1})] - P_w(C_{c1} + A_{c1}) + P_w\int_0^1 C_1^{II}(X^{II})dX^{II} = 0 \tag{A3f}$$

$$C_0^I(0) = \gamma_1 \tag{A3g}$$

$$C_0^{II}(1) = \gamma_2 \tag{A3h}$$

$$-(24\alpha L_1^2\mu/h_1^3)\int_0^1 V_0^I(X^I)dX^I - (24\alpha L_2^2\mu/h_2^3)\int_0^1 V_0^{II}(X^{II})dX^{II} = \Delta p(\text{hydrostatic}) + RTT_0\nu\{\sigma_{TJ}[\gamma_1 - C_1^{II}(0)] + \gamma_Z\} \tag{A3i}$$

$$C_0^I(1) = C_0^{II}(0) \tag{A3j}$$

$$L_1(-\eta_1\nu dC_1^I(X^I)/dX^I + V_0^I(X^I)]_{x^I=1} = L_2[-\eta_2\nu dC_1^{II}(X^{II})/dX^{II} + V_0^{II}(X^{II})]_{x^{II}=0} \tag{A3k}$$

$$L_1V_0^I(1) = L_2V_o^{II}(0) \tag{A3l}$$

where $K^2 = 1/(\eta_2\nu)$, $\gamma_1 = (\Gamma_1^* - \Gamma_2^*)/(2\nu\Gamma_0)$, $\gamma_2 = -\gamma_1$, and $\gamma_z = Z_1^*/(\nu\Gamma_0)$.

We solve this complex set of differential-integral equations by first integrating Eq. A3a-A3d to find that

$$\begin{aligned} C_1^I(X^I) &= (A_1 - A_3)X^I/(\eta_1\nu) + A_4 \\ V_0^I(X^I) &= A_1 \\ C_1^{II}(X^{II}) &= kB_1\cosh(KX^{II}) + KB_2\sinh(KX^{II}) - 1 + C_{c1} + A_{c1} \\ V_0^{II}(X^{II}) &= B_1\sinh(KX^{II}) + B_2\cosh(KX^{II}) - X^{II} + A_2 \end{aligned} \tag{A4}$$

where the six unknown integration constants A_1, A_2, A_3, A_4, B_1, and B_2 as well as the still unknown C_{c1} and A_{c1} are to be determined by substituting Eq. A4 into the remaining eight Eq. A3e–A3l and then simultaneously solving them. Eqs. A3g, A3k, A3l simplify to

$$A_4 = \gamma_1$$

$$A_3L_1 = L_2A_2$$

$$L_1A_1 = L_2(B_2 + A_2)$$

so that $A_2 = (L_1/L_2)A_1 - B_2$ and $A_3 = A_1 - (L_2/L_1)B_2$. When these expressions are substituted into Eqs. A3f, A3h, A3j, the latter can be solved to obtain

$$C_{T1} = C_{c1} + A_{c1} = (1/D)\{K(C-1) + ES - KC(C-1) + KS^2 - EKC - K^2S + \gamma_2[K(C-1) + ES] - \gamma_1[KC(C-1) - KS^2] + W_\gamma(EKC + K^2S)\}$$

$$B_1 = (1/D)[(E + KS)(1 + W) + (C-1)(\gamma_1 - \gamma_2) - W_\gamma(E + KS) + W(E\gamma_2 + KS\gamma_1)]$$

$$B_2 = (1/D)[K(1 - C - WC + W) + \gamma_2(S + WK) - \gamma_1(S + WKC) - W_\gamma(K - KC)]$$

where $S = \sinh(K)$, $C = \cosh(K)$, $E = L_2/(L_1\eta_1\nu)$, $W = \sqrt{3}\ d(P_{W1} + P_{W2})/(8L_2P_W)$, $W_\gamma = \sqrt{3}\ d[P_{W1}(\gamma_1 + \gamma_Z) + P_{W2}\gamma_2]/(8L_2P_W)$ and $D = -K + 2KC - KC^2 + KCWE + KS^2 + K^2SW + ES$. These results can now be inserted into Eq. A3i to find that

$$A_1 = [0.5 - \Delta p(\text{hydrostatic})h_2^3/(24\mu\alpha L_2^2) - B_1(C-1)/K - B_2(S/K - 1) + \theta]/[L_1/L_2 + (L_1/L_2)^2/(h_1/h_2)^3]$$

where $\theta = -RT\Gamma_0\nu h_2^3\ [\gamma_Z + \sigma_{TJ}(\gamma_1 - KB_1 + 1 - C_{c1} - A_{c1})\ ]/(24\mu\alpha L_2^2)$. Eq. A3e can now be combined with the previously calculated C_{T1} value to find that $C_{c1} = (\xi_1 C_{T1} - \xi_3)/(\xi_1 - \xi_2)$

and

$$A_{c1} = C_{T1} - C_{c1}$$

where $\xi_1 = -(P_s + \alpha)/\alpha$, $\xi_2 = \sqrt{3}\ d(\alpha_1 + \alpha_2 + P_{s1} + P_{s2})/(8L_2\alpha) - 1$, and $\xi_3 = (P_s + \alpha)\ [B_1S + B_2(C-1) - 1]/\alpha + \sqrt{3}\ d\ (P_{s1}\gamma_1 + P_{s2}\gamma_2)/(8L_2\alpha)$.

The solution could be continued to greater accuracy by examining the coefficients of order ν^2. That set of differential-integral equations is highly nonlinear and cannot be integrated analytically. However, it is not necessary to solve for these next higher order terms because it is quite accurate to truncate the series (Eq. A1) after the first-order terms. This can be demonstrated by noting that the terms neglected in eqs. A4, e.g. $V_1(X)\ C_1(X)$, act as source terms creating (or destroying) solute in the extracellular channel. Thus, the discrepancy between the net solute flux, J_s (net, $X^I = 0$), at the apical cell border and the net solute flux, J_s (net, $X^{II} = 1$), at the basal cell border provides an estimate of these sourcelike error terms. For our model of the corneal endothelium, under the various boundary condition in Figs. 4–8 this flux error is 2 to 4%.

From these results we can now compute the solute (J_s) and water (J_v) fluxes per cell through the cell and channel at the apical ($X^I = 0$) and basal ($X^{II} = 1$) cell margins:

$$J_s(\text{cell}, X^I = 0) = (3\sqrt{3}d^2/8)\quad [P_{s1}(\Gamma_1^* - C_c^*) - \alpha_1 C_c^*]$$

$$= (3\sqrt{3}d^2/8)(\Gamma_0\alpha/P_s)[P_{s1}\nu\ (\gamma_1 - C_{c1}) - \alpha_1\ (1 + \nu C_{c1})\ ]$$

$$J_s(\text{channel}, X^I = 0) = (3dh_1/2)(-D\ dC^*/dX^* + V^*C^*) = 3d\alpha L_1\Gamma_0 A_3$$

$$J_s(\text{cell}, X^{II} = 1) = (3\sqrt{3}d^2/8)\ [-P_{s2}\ (\Gamma_2^* - C_c^*) + \alpha_2 C_c^*]$$

$$= (3\sqrt{3}d^2/8)\ (\Gamma_0\alpha/P_s)\ [P_{s2}\nu(C_{c1} - \gamma_2) + \alpha_2(1 + \nu C_{c1})\ ]$$

$$J_s(\text{channel}, X^{II} = 1) = (3dh_2/2)\ [-D\ dC^*/dX^* + V^*\ C^*) = 3d\alpha L_2\Gamma_0(A_2 - 1)$$

$$J_v(\text{cell}, X^I = 0) = (-3\sqrt{3}\ d^2P_{w1}/8)\ [\Gamma_1^* + Z_1^* - C_c^* - A_c^*]$$

$$= (-3\ \sqrt{3}\ d^2P_{w1}\Gamma_0\nu/8)\ (\gamma_1 + \gamma_z - C_{c1} - A_{c1})$$

$$J_v(\text{channel}, X^I = 0) = 3dh_1V^*/2 = 3d\alpha L_1A_1$$

$$J_v(\text{cell}, X^{II} = 1) = (3\sqrt{3}d^2P_{w2}/8)\ (\Gamma_2^* - C_c^* - A_c^*)$$

$$= (3\sqrt{3}d^2P_{w2}\Gamma_0\nu/8)\ (\gamma_2 - C_{c1} - A_{c1})$$

$$J_v(\text{channel}, X^{II} = 1) = 3dh_2V^*/2 = 3d\alpha L_2\ (B_1S + B_2C - 1 + A_2)$$

where half the flux through each facet of the six-sided channel has been assigned to each of the two bordering cells. The net solute and water fluxes across the entire cell layer are given by

$$J_s(\text{net}, X^I = 0) = J_s(\text{cell}, X^I = 0) + J_s(\text{channel}, X^I = 0)$$

$$J_s\,(\text{net}, X^{II} = 1) = J_s\,(\text{cell}, X^{II} = 1) + J_s\,(\text{channel}, X^{II} = 1)$$

$$J_v\,(\text{net}, X^{I} = 0) = J_v\,(\text{cell}, X^{I} = 0) + J_v\,(\text{channel}, X^{I} = 0)$$

$$J_v\,(\text{net}, X^{II} = 1) = J_v\,(\text{cell}, X^{II} = 1) + J_v\,(\text{channel}, X^{II} = 1)$$

where J_v (net, $X^I = 0$) is identically equal to J_v (net, $X^{II} = 1$) but (as noted above) if the series (Eq. A1) is truncated after the first-order terms, then J_s (net, $X^I = 0$) equals J_s (net, $X^I = 0$) to within order (ν).

We would like to thank Dr. Peter Reinach, Mr. John Durham, Dr. William Brodsky, Dr. Patrick Eggena, Dr. Jorge Fischbarg, and Dr. Jong J. Lim for helpful discussions.

The numerical calculations were performed on the Tektronix 4051 of the Department of Physiology, The Mount Sinai School of Medicine with additional support from The City University Computing Center and on Dr. Fischbarg's PDP 11/34 at the Department of Ophthalmology Research, Columbia University.

Dr. Liebovitch was supported by grants EY 07014, EY 07002, Ey 01080 from the National Institutes of Health. Dr. Weinbaum received a Faculty Research Award Program award from the City University of N. Y.

Received for publication 13 November 1980 and in revised form in April 1981.

REFERENCES

1. Berridge, M. J., and J. L. Oschman. 1972. Transporting Epithelia. Academic Press, Inc., New York.
2. House, C. R. 1974. Water Transport in Cells and Tissues. Edward Arnold Ltd., London, England.
3. Gupta, B. L., R. M. Moreton, J. L. Oschman, and B. J. Wall, editors. 1977. Transport of Ions and Water in Animals. Academic Press, Inc., New York.
4. Skadhauge, E. 1977. Analysis of Computer Models in Transport of Ions and Water in Animals. B. L. Gupta, J. L. Oschman, R. B. Moreton, B. J. Wall, editors. Academic Press, Inc., New York.
5. Kedem, O., and A. Katchalsky. 1958. Thermodynamic analysis of biological membranes to non-electrolytes. Biochim. Biophys. Acta. 27:229–246.
6. Katchalsky, A., and P. F. Curran. 1975. Nonequilibrium Thermodynamics in Biophysics, Harvard University Press, Cambridge, Mass.
7. Curran, P. F. 1960. Na, Cl, and water transport by rat ileum in vitro. *J. Gen. Physiol.* 43:1137–1148.
8. Patlak, C. S., D. A. Goldstein, and J. F. Hoffman. 1963. The flow of solute and solvent across a two-membrane system. *J. Theor. Biol.* 5:426–442.
9. Kaye, G. I., H. O. Wheeler, R. T. Whitlock, and N. Lane. 1966. Fluid transport in the rabbit gall bladder. A combined physiological and electron microscopic study. *J. Cell Biol.* 30:237–268.
10. Spring, K. R. 1973. A parallel path model for Necturus proximal tubule. *J. Membr. Biol.* 13:323–352.
11. Sackin, H., and E. L. Boulpaep. 1975. Models for coupling of salt and water transport. *J. Gen. Physiol.* 66:671–733.
12. Boulpaep, E. L., and H. Sackin. 1977. Role of the paracellular pathway in isotonic fluid movement across the renal tubule. *Yale J. Biol. Med.* 50:115–131.
13. Diamond, J. M., and W. H. Bossert. 1967. Standing gradient osmotic flow. A mechanism for coupling of water and solute transport in epithelia. *J. Gen. Physiol.* 50:2061–2083.
14. Diamond, J. M., and W. H. Bossert. 1968. Functional consequences of ultrastructural geometry in "backwards" fluid transporting epithelia. *J. Cell Biol.* 37:694–702.
15. Weinbaum, S. and J. R. Goldgraben. 1972. On the movement of water and solute in extracellular channels with filtration, osmosis and active transport. *J. Fluid Mech.* 53:481–512.
16. Schafer, J. A., C. S. Patlak, and T. E. Andreoli. 1975. A component of fluid absorption linked to passive ion flows in the superficial pars recta. *J. Gen. Physiol.* 66:445–471.
17. Schafer, J. A., C. S. Patlak, and T. E. Andreoli. 1977. Fluid absorption and active and passive ion flows in the rabbit superficial pars recta. *Am. J. Physiol.* 233:F154–F167.
18. Andreoli, T. E., and J. A. Schafer. 1978. Volume absorption in the pars recta III. Luminal hypotonicity as a driving force for isotonic volume absorption. *Am. J. Physiol.* 234:F349–F355.
19. Andreoli, T. E., and J. A. Schafer. 1979. External solution driving forces for isotonic fluid absorption in proximal tubules. *Fed. Proc.* 38:154–160.

20. Huss, R. E., and J. L. Stephenson. 1979. A mathematical model of proximal tubule absorption. *J. Membr. Biol.* 47:377–399.
21. Weinstein, A. M., and J. L. Stephenson. 1979. Electrolyte transport across a simple epithelium, steady state and transient analysis. *Biophys. J.* 27:165–186.
22. Marsh, D. J., and R. E. Huss. 1979. A model of pressure-modulated fluid reabsorption by the renal proximal tubule: implications for glomerulotubular balance. *Fed. Proc.* 38:2037–2042.
23. Weinbaum, S. 1977. A cellular conservation model for the replenishment of water and solute in epithelia with local osmotic transport. *ASME Third Biomech. Symp.*, Yale University, New Haven, Conn. AMD. 23:75–79.
24. Goldgraben, J. R., and S. Weinbaum. 1973. On the mixing of a low Reynolds number biological jet with a quiescent outer bathing solution. *J. Fluid Mech.* 59:159–175.
25. Keller, K. H., and T. R. Stein. 1967. A two dimensional analysis of porous membrane transport. *Math. Biosci.* 1:421–437.
26. Segel, L. A. 1970. Standing-gradient flows driven by active solute transport. *J. Theor. Biol.* 29:233–250.
27. Duke-Elder, S., and J. Gloster. 1969. The Physiology of the Eye and of Vision. *In* System of Opthalmology. Vol. 4. Sir Stewart Duke-Elder, editor. The C.V. Mosby Co., St. Louis, Mo. 337–359.
28. Maurice, D. M. 1969. The cornea and sclera. *In* The Eye, Vol. 2, 2nd edition. H. Davson, editor. Academic Press, Inc., New York. 489–600.
29. Elliott, G. F., J. M. Goodfellow, and A. E. Woolgar. 1980. Swelling studies of bovine corneal stroma without bounding membranes. *J. Physiol. (Lond.)*. 298:453–470.
30. Hebys, B. O., S. Mishima, and D. M. Maurice. 1963. The imbibition pressure of the corneal stroma. *Exp. Eye Res.* 2:99–111.
31. Hedbys, B. O., and C. H. Dohlman. 1963. A new method for the determination of the swelling pressure of the corneal stroma in vitro. *Exp. Eye Res.* 2:122–129.
32. Fatt, I., and T. K. Goldstick. 1965. Dynamics of water transport in swelling membranes. *J. Colloid Sci.* 20:962–989.
33. Mishima, S., and T. Kudo. 1967. In vitro incubation of rabbit cornea. *Invest. Opthalmol.* 6:329–339.
34. Maurice, D. M. 1972. The location of the fluid pump in the cornea. *J. Physiol.* 221:43–54.
35. Fischbarg, J., C. R. Warshavsky, and J. J. Lim. 1977. Pathways for hydraulically and osmotically-induced water flows across epithelia. *Nature (Lond.)*. 226:71–74.
36. Fischbarg, J. 1978. Fluid transport by corneal endothelium. *In* Comparative Physiology: Water, Ions and Fluid Mechanics. K. Schmidt-Nielsen, L. Bolis, and S. H. P. Maddrell, editors. Cambridge University Press, London, England. 21–39.
37. Duke-Elder, S., and K. C. Wybar. 1961. System of Ophthalmology. *In* Anatomy of the Visual System, Vol. 2. Sir Stewart Duke-Elder, editor. The C. V. Mosby Company, St. Louis, Mo. 109–113.
38. Kaye, G. I., and G. D. Pappas. 1962. Studies on the cornea I. *J. Cell Biol.* 12:457–479.
39. Iwamoto, T., and G. K. Smelser. 1965. Electron microscopy of the human corneal endothelium with reference to transport mechanisms. *Invest. Ophthalmol.* 4:270–284.
40. Hogan, M. J., J. A. Alvarado, and J. E. Weddell. 1971. Histology of the Human Eye. W. B. Saunders Company, Philadelphia, Pa. 102–109.
41. Capella, J. A., H. F. Edenhauser, and D. L. van Horne, editors. 1973. Corneal Preservation. Charles C. Thomas, Publisher. Springfield, Illinois.
42. Kikkawa, Y. 1966. Corneal potential studies on whole eye. *Exp. Eye Res.* 5:21–30.
43. Green, K. 1967. Solute movement across the constituent membranes of the cornea. *Exp. Eye Res.* 6:79–92.
44. Fischbarg, J. 1972. Potential difference and fluid transport across rabbit corneal endothelium. *Biochim. Biophys. Acta.* 288:362–366.
45. Fischbarg, J., and J. J. Lim. 1973. Determination of the impedance locus of corneal endothelium. *Biophys. J.* 13:595–599.
46. Fischbarg, J. 1973. Active and passive properties of the rabbit corneal endothelium. *Exp. Eye Res.* 15:615–638.
47. Fischbarg, J., and J. J. Lim. 1974. Role of cations, anions and carbonic anhydrase in fluid transport across rabbit corneal endothelium. *J. Physiol. (Lond.)*. 241:647–675.
48. Barfort, P. and D. Maurice. 1974. Electrical potential and fluid transport across the corneal endothelium. *Exp. Eye Res.* 19:11–19.
49. Hodson, S. 1974. The regulation of corneal hydration by a salt pump requiring the presence of sodium and bicarbonate ions. *J. Physiol. (Lond.)*. 236:271–302.
50. Hodson, S., and F. Miller. 1976. The bicarbonate ion pump in the endothelium which regulates the hydration of rabbit cornea. *J. Physiol. (Lond.)*. 263:563–577.

51. Kaye, G. I., R. C. Sibley, and F. B. Hoefle. 1973. Recent studies on the nature and function of the corneal endothelial barrier. *Exp. Eye Res.* 15:585–613.
52. Leuenberger, P. M. 1973. Lanthanium hydroxide tracer studies on rat corneal endothelium. *Exp. Eye Res.* 15:85–91.
53. Bowman, K. A., and K. Green. 1976. Hydrostatic pressure effects on deswelling of de-epithelialized and de-endothelialized corneas. *Invest. Opthalmol.* 15:546–550.
54. Shapiro, M. P., and O. A. Candia. 1973. Corneal hydration and metabolically dependent transcellular passive transfer of water. *Exp. Eye Res.* 15:659–666.
55. Rehm, W. S., and S. G. Spangler. 1976. A new theory for the mechanism by which the endothelium controls corneal hydration. *Ala. J. Med. Sci.* 13:196–205.
56. Rhem, W. S., and S. G. Spangler. 1977. A theory of endothelial control of corneal hydration. *Am. J. Optom. Physiol. Opt.* 54:439–444.
57. Lim, J. J., and J. Fischbarg. 1976. Standing-gradient flow – examination of its validity using an analytic method. Biochim. Biophys. Acta. 443:339–347.
58. Friedman, M. H. 1972. A quantitative description of equilibrium and homeostatic thickness regulation in the vivo cornea I. Normal cornea. *Biophys. J.* 12:648–6665.
59. Friedman, M. H. 1972. A quantitative description of equilibrium and homeostatic thickness regulation in the in vivo cornea II. Variations from the normal state. *Biophys. J.* 12:666–682.
60. Friedman, M. H. 1973. Unsteady transport and hydration dynamics in the in vivo cornea. *Biophys. J.* 13:890–910.
61. Friedman, M. H. 1973. Unsteady aspects of corneal thickness control. *Exp. Eye Res.* 15:645–658.
62. Klyce, S. D., and S. R. Russel. 1979. Numerical solution of coupled transport equations applied to corneal hydration dynamics. *J. Physiol. (Lond.).* 292:107–134.
63. Green, K., and M. A. Green. 1969. Permeability to water of rabbit corneal membranes. *Am. J. Physiol.* 217:635–641.
64. Green, K., and S. J. Downs. 1976. Corneal membrane water permeability as a function of temperature. *Invest. Ophthalmol.* 15:304–307.
65. Stanley, J. A., S. Mishima, and S. D. Klyce. 1966. In vivo determination of endothelial permeability to water. *Invest. Opthalmol.* 5:371–377.
66. Mishima, S., and B. O. Hedbys. 1967. The permeability of the corneal epithelium and endothelium to water. *Exp. Eye Res.* 6:10–32.
67. Maurice, D. M. 1951. The permeability to sodium ions of the living rabbit's cornea. *J. Physiol. (Lond.).* 112:367–391.
68. Trenberth, S. M., and S. Mishima. 1968. The effect of ouabain on the rabbit corneal endothelium. *Invest. Opthalmol.* 7:44–52.
69. Kim, J. H., K. Green, M. Martinez, and D. Paton. 1971. Solute permeability of the corneal endothelium and descemet's membrane. *Exp. Eye Res.* 12:231–238.
70. Hull, D. S., K. Green, M. Boyd, and H. Wynn. 1977. Corneal endothelium bicarbonate transport and the effect of carbonic anhydrase inhibitors on endothelial permeability and fluxes and corneal thickness. *Invest. Opthalmol. Visual. Sci.* 16:883–892.
71. Green, K., J. G. Buyer, and D. S. Hull. 1978. Corneal endothelial bicarbonate fluxes following preservation in solutions of varying compositions. *Invest. Opthalmol. Visual. Sci.* 17:1117–1121.
72. Pappenheimer, J. R., E. M. Renkine, and L. M. Borrero. 1951. Filtration, diffusion and molecular sieving through capillary membranes. *Am J. Physiol.* 167:13–46.
73. Perl, W. 1971. Modified filtration permeability model of transcapillary transport – a solution of the Pappenheimer pore puzzle? *Microvasc. Res.* 3:233–251.
74. Curry, F. E. 1974. A hydrodynamic description of the osmotic reflection coefficient with application to the pore theory of transcapillary exchange. *Microvasc. Res.* 8:236–252.
75. Ganatos, P., S. Weinbaum, J. Fischbarg, and L. Liebovitch. 1980. A hydrodynamic theory for determining the membrane coefficients for the passage of spherical molecules through an intercellular cleft. *Adv. in Bioeng.* (ASME) 193–199.
76. Hoffmann, E. K. 1977. Control of cell volume. *In* Transport of Ions and Water in Animals. B. L. Gupta, J. L. Oschman, R. B. Moreton, and B. J. Wall, editors. Academic Press, Inc., New York. 285–332.
77. Rich, G. T., R. J. Sha'afi , T. C. Barton, and A. K. Solomon. 1967. Permeability studies on red cell membranes of dog, cat and beef. *J. Gen. Physiol.* 50:2391–2405.
78. Zadunaisky, J. A., M. N. Parisi, and R. Montoreano. 1963. Effect of antidiuretic hormone on the permeability of single muscle fibers. *Nature (Lond.).* 200:365–366.

79. Fischbarg, J. 1981. The paracellular pathway in the corenal endothelium. *Proc. Macy Conf. Paracellular Pathway*. S. Bradley, editor. In press.
80. Stein, W. D. 1967. The Movement of Molecules Across Cell Membranes. Academic Press, Inc., New York. 94–99.
81. Kaye, G. I., J. D. Cole, and A. Donn. 1965. Electron microscopy: sodium localization in normal and ouabain-treated transporting cells. *Science. (Wash. D.C.)*. 150:1167–1168.
82. Kaye, G. I., and L. W. Tice. 1966. Studies on the cornea V. Electron microscopic localization of adenosine triphosphatase activity in the rabbit cornea in relation to transport. *Invest. Ophthalmol.* 5:22–32.
83. Leuenberger, P. M., and A. B. Novikoff. 1974. Localization of transport adenosine triphosphatase in rat cornea. *J. Cell Biol.* 60:721–731.